World Journal of Advanced Research and Reviews
eISSN: 2581-9615 CODEN (USA): WJARAI
Cross Ref DOI: 10.30574/wjarr
Journal homepage: https://wjarr.com/

(RESEARCH ARTICLE)

Check for updates

Computational fluid dynamics (CFD) of a three-inlet-Y-junction duct connected to a U-bend: Influence of inlet velocities on air and water flows subjected to cold fronts and turbulence

Pape Tamsir Ndiaye [1,*], Goumbo Ndiaye [2], Omar Ngor Thiam [1,3], Momath Ndiaye [1,4] and Oumar Drame [1,3]

[1] *Fluid Mechanics and Transfer Laboratory, Department of Physics, Sciences and Technologies Faculty, Cheikh Anta DIOP University, Dakar-Fann, Senegal.*
[2] *The Water, Energy, Environment and Industrial Processes Laboratory of the Polytech Higher School, Cheikh Anta Diop University, Dakar, Senegal.*
[3] *Research Group on Solar Energy and Transfers (GREST), Sciences and Technologies Faculty, Cheikh Anta DIOP University, Dakar-Fann, Senegal.*
[4] *Department of the Ufr Hydraulics, Rural Engineering, Machinery and Renewable Energy,University of Sine Saloum Elhadji Ibrahima NIASS, Kaolack, Senegal.*

World Journal of Advanced Research and Reviews, 2025, 27(02), 680-692

Publication history: Received on 30 June 2025; revised on 09 August 2025; accepted on 11 August 2025

Article DOI: https://doi.org/10.30574/wjarr.2025.27.2.2838

Abstract

This study presents the movement of air and water flowing in a Y-junction duct with three connected inlets of a U-bend with attention to the impact of cold fronts. Analyses were carried out to observe the behavior of the fluids (air and water) at the duct axis, after the mixing zone (at 70 mm), just upstream of the bend and downstream, at the outlet. The realizable k-ε viscous turbulence model coupled with the energy equation were solved numerically using Ansys Fluent 2024R2. Three cases of cold front formation were studied according to the inlet velocities. An extended cold front appears when the cold fluid enters slowly from inlets 2 and 3, while a high velocity at inlet 1 (case II) can extend the front to outlet CS3. The U-bend acts as a turbulence amplifier, but the response of the fluid in question (air and water) depends both on their physical properties (density, kinematic viscosity, and inertia) and their physicochemical characteristics. The complex dynamics of these flows are explained not only by mechanical phenomena but also by intermolecular interactions: water (a polar molecule), capable of forming hydrogen bonds and susceptible to cold fronts, reacts differently from air, a mixture of non-polar gases with weak intermolecular interactions.

Keywords: Ansys Fluent; Air and water movement; CFD; Heat and mass transfer; realizable k-ε turbulence model; T-Junction; U-bend

1. Introduction

Essential to achieving optimal thermal comfort and acceptable indoor air quality, the mixing of air at different temperatures is an important issue. In heating, ventilation, and air conditioning (HVAC), air quality control considers the mastery of the movement of hot and cold air essential. Also, the mixing of water at different temperatures is considered during the construction of wastewater treatment plants, water treatment, and hydraulic engineering. The shape of ducts, tubes, channels, conduits, channels, and vents plays a major role in air and water dynamics for achieving acceptable indoor air or water quality, hot air control, wastewater management, plant construction, water treatment, and hydraulic engineering. Whenever it is necessary to divide or combine flows, joints (T, Y, etc.) are used in the main piping systems.

* Corresponding author: Pape Tamsir Ndiaye

Along with joints, many other obstacles such as valves, turbines, pumps, elbows, elbow-junctions, contractions, expansions, meters may be present. They affect the overall efficiency by causing major and minor losses in the pipes. A lot of work on junctions of experimental and numerical CFD setups with tools such as ANSYS FLUENT, OPENFOAM are used for this purpose [1-16].

Athulya A. Sa et al. [1] presented a multiphase flow model through the T-junction and the phase redistribution phenomenon at the junction using ANSYS FLUENT software. Based on their study, the following conclusions were drawn: it can be seen that a larger amount of air pocket is formed in the lower part of the bypass arm, phase separation is negligible in the bypass arm due to the effect of gravity and by analyzing the multiphase flow, they saw that considering the fluid alone, phase separation is greater at the outlet than at the junction.

Nimadge Mr.G.B. et al. [2] set the goal to study the steady and incompressible flow of a fluid through a T-junction and to get familiar with CFD by focusing on losses in piping systems, as the working fluid through pipes plays an important role in the operation of industries such as chemical industries, petroleum industries, etc. They prepared an experimental setup to obtain the reference data when the fluid passes through the T-junction of the pipe, the same data is used for CFD analysis using software such as ANSYS FLUENT.

Khan Wasim et al. [3] numerically studied the plug formation mechanism during gas-liquid two-phase flow in a T-junction microchannel by developing a two-dimensional (2D) model of the microchannel using ANSYS Academic Research CFD 18.2 software and adopting the volume of fluid (VOF) method to solve it. Their obtained results agree well with the experimental results. The plug length, pressure drop, and velocity variations inside the plugs were measured under different operating conditions. The effects of contact angle (0°–155°), fluid viscosity, and surface tension on the two-phase flow interaction parameters, as well as the effect of gas and liquid superficial velocities, were examined in detail. They found that the liquid film formed at low capillary count (Ca) was very thin and was observed only for fine meshes near the channel wall.

DOROSHENKO Yaroslav et al. [4] carried out 3D modeling of the elbow and T-junction in the linear part of the gas pipeline, especially at the places where a complex movement of multiphase flows occurs and changes its direction. Based on the Lagrangian approach (Discrete Phase Model - DPM), numerical modeling methods were developed to simulate the multiphase flow movement in the elbow and T-junction of the linear part of the gas pipeline using the ANSYS Fluent R17.0 Academic software package. The mathematical model is based on solving the Navier-Stokes equations and closed discrete phase continuity and motion equations with the Launder-Sharma two-parameter turbulence model (k-e) with appropriate initial and boundary conditions. These results provide the opportunity for a comprehensive and in-depth study of the erosive wear of the elbow and T-junction of the linear part of the gas pipeline and adjacent pipeline sections, as well as an assessment of their strength and residual life. The velocity of liquid and solid particles, the impact angles, the diameters of condensed droplets and solid particles at the collision site were determined. Such studies open the prospect of a comprehensive and in-depth research on the erosive wear of elbows and T-junctions in the linear section of gas pipelines.

RAID AHMED MAHMOOD [5] presented a CFD simulation study to predict and visualize the separation of two-phase flows in the vertical T-junction and a comparison between the CFD results and the associated experimental results to validate their CFD results. Using ANSYS 17.1 to perform the simulation, the geometry of the T-junction was generated by ANSYS modular design based on the dimensions of the experimental test section and then passed to the ANSYS mesh to generate a suitable mesh.

A numerical study in a three-inlet Y-junction microchannel was carried out with two different numerical codes: ANSYS Fluent and Open-FOAM by Chiriac Eugen et al. [6]. Using the same inlet and boundary conditions, three main parameters are studied: velocity amplitude, pressure and vorticity amplitude. The microchannel was fabricated using PDMS (Polydimethylsiloxane) soft litography and were used for the validation of numerical simulations. The simulation results were analyzed and a comparison between the numerical codes was carried out with the aim of testing the capabilities of the two numerical codes in a simulation of flow mixing in a microchannel.

Makarem M. A. [7] proposed a CFD simulation of CO2 capture in a microchannel by aqueous mixtures of MEA and [Bmim] BF4 modified with TiO2 nanoparticles as chemical additives. The flow hydrodynamics, mass transfer characteristics and CO_2 absorption performance of the proposed solvent were investigated in a T-shaped microchannel structure by steady-state computational fluid dynamics technique. To present a detailed model, the Navier-Stokes and continuity equations are combined with a two-phase laminar flow module accounting for mass transfer between heterogeneous phases. The effects of [Bmim]BF_4 and TiO_2 mass fractions on CO_2 loading, bubble formation, and velocity profile were then studied at different gas and liquid holdups, with an ionic liquid fraction ranging from 0% to 10% and

a nanoparticle fraction ranging from 0% to 0.1%. According to their simulation results, the solvent containing 10% [Bmim]BF4, 3% MEA, and 0.04% TiO2 exhibited the maximum purification fraction of 79.62%.

Taha Enas Salman et al. [8] examined the influence of turbulent parameters on the characteristic centerline of a fluid flow through a T-junction connected to a Venturi tube via a pipe. The continuity equation, momentum equation and energy equation of water are modeled and solved using ANSYS FLUENT 2020R1 software while for turbulence, the standard type turbulent model (k-ε) is used. The model is obtained on the velocity distribution, pressure drop distribution, turbulent kinetic energy and turbulent dissipation rate. The results showed a divergence in the values of the effect of the T-junction on the Venturi meter regarding the velocity distribution and pressure drop, while they showed a similar behavior for the turbulence parameters.

A three-dimensional (3D) numerical simulation of a liquid/liquid two-phase flow was carried out in a rectangular microchannel with a T-junction by SAID Mohammed et al. [9]. They used the volume of fluid (VOF) method with ANSYS Fluent to capture the interface between the two phases and the dynamic mesh adaptation technique along with the assumption of a symmetry plane helped them reduce the computational cost. Their study focused on the flow patterns and hydrodynamics of plugs and their results revealed six distinct flow patterns by dispersing water in a continuous silicone oil phase. By decreasing the flow rate ratio as well as the viscosity ratio, the liquid film thickness increases in the corners and side planes. In turn, this has a significant impact on the liquid film velocity and the plug velocity.

Bushra Khatoon et al. [10] conducted numerical and experimental studies for the analysis of hydrodynamics and volumetric mass transfer coefficient in a cross-T junction microchannel for a two-phase gas-liquid flow system. Initially, the CO2-water hydrodynamic simulation was performed using ANSYS-FLUENT 2021 R2 with the fluid volume technique. The computational fluid dynamics model was validated by comparing the results with experimental data. The results obtained in numerical simulation and experimental work show that the total volumetric mass transfer coefficient (margin 0.1–0.8 1/s) increases with increasing gas velocity, but it decreases with increasing film thickness (0.01–0.05 mm) and temperature (T = 298.15 K and 303.15 K). It was observed that with increasing bubble velocities, the total mass transfer coefficient also increases, and with increasing film thickness, it shows the opposite effect due to the dominant parameters in the microchannel, i.e., surface tension.

Wang Fuzhang et al. [11] presented a paper on the dynamics of unsteady air and water through a three-inlet T-shaped duct, focusing on the problem of cold fronts. They performed simulations to notice the nature of these fluids some distances after mixing (70 mm), before turning the duct and after turning the duct. They solved the feasible k-ε viscous model and energy equation numerically using Ansys Fluent 2022R1. The examination of residual independence and meshing was taken into account to check the convergence of the results. Considering the variation of inlet velocity, they examined three cases of cold front formation. When the inlet velocities of cold air/water and warm air/water are the same, the formation of the cold front is invisible at the early stage despite the fact that air flows faster than water. They found that the optimal average vortex kinetic energy per unit mass formed near the T-junction, not due to previously formed cold fronts, but due to the pressure recirculation at the bend affecting the velocity of the cold fluid substance coming from the two adjacent inlets (i.e., Inlet 2 and Inlet 3).

However, like Wang Fuzhang et al. [11], we propose a CFD study and a comparative analysis between the dynamics of air and water through a Y-junction duct (not T-junction unlike Wang Fuzhang et al. [11]) followed by a three-inlet U-bend where mixing and cold fronts start at 70 mm from the three inlets. We will study the effects of the variation of the three inlet velocities of the fluids (air and water) cold or hot on the flow and the overall dynamics (velocity field, pressure variations, temperature and turbulence) and how they vary in the duct at a distance after mixing, before the bend and after the bend and affect the formation and evolution of cold fronts. We will also emphasize the difference between air and water.

2. Mathematical Formulation

2.1. Description of the physical model and simplifying assumptions:

In this work, we considered two circular aluminum ducts of 40 mm diameter, where it was assumed that air and water circulate separately in each of the ducts in a Y-junction shape with three inlets followed by a U-bend. As shown in Figure 1, the mixing zone is located 70 mm from inlets 1, 2 and 3 in each of these ducts. The geometric structure in 3D mode, presents a circular surface (CS1) located 30 mm from the mixing domain, another circular surface located 100 mm from the mixing domain (CS2) and an outlet located 20 mm from the duct bend (CS3). The hot fluid (air or water) enters the domain through inlet 1 with a velocity InV1 and a temperature of 30 °C, while the cold fluid inlets are located through inlets 2 and 3 with velocities InV2 and InV3 at 5 °C, respectively. The physical properties of fluids are listed in Table 1.

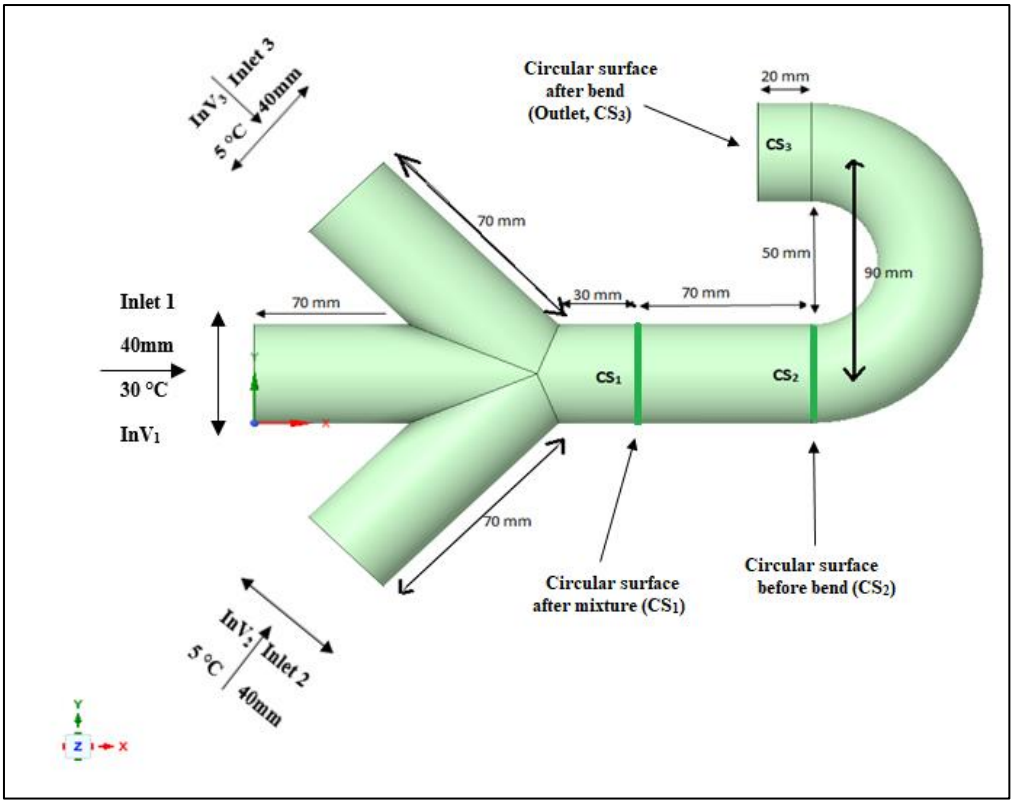

Figure 1 Illustration of the geometric model (three-way Y-junction followed by a U-bend)

Table 1 The physical properties of the fluid considered : air and liquid water

	Air	**liquid water**
Density ρ : [Kg/m^3]	1.225	998.2
Viscosity μ : [Kg/(m.s)]	1.7894-× 10^{-5}	1.003× 10^{-3}
Thermal Conductivity k : [W/(m.K)]	0.0242	0.6
Specific Heat Cp : [J/(Kg.K]	1006.43	4182

To carry out this work, we admit some simplifying hypotheses such as: the fluids (water and air) are incompressible and Newtonian, the physical properties are quasi-constant, there is no phase change and the flow is fully turbulent and permanent.

2.2. Governing equations

Although Reynolds Averaged Navier-Stokes (RANS) models have some limitations but deserve to be recognized as the most reliable for characterizing velocity fields of turbulent flows due to near-wall modeling, turbulence modeling (i.e., involving averaging the equations governing fluid motion over time or space to obtain an average flow field and additional terms representing turbulence effects), reliable for higher Reynolds numbers, inherently assumes that turbulent fluctuations can be decomposed into an average and fluctuating component, with the fluctuations decaying rapidly toward zero. Moreover, RANS provides reasonable results when interactions, separation, and recirculation are simple [12-13]. In this study, the feasible k-ε viscous model of RANS by Shih et al. [14] considered the eddy viscosity not as a constant, but as a function depending on the angular rotational velocity of the system, the average deformation and rotational velocities, as well as the turbulence properties (k and ε).

The continuity (1.a) and momentum (1.b) equations of averaged Navier-Stokes called RANS are as follows:

$$\begin{cases} \dfrac{\partial \bar{u}_i}{\partial x_i} = 0 \\ \dfrac{\partial}{\partial t}\left(\rho \bar{u}_i\right) + \dfrac{\partial}{\partial x_i}\left(\rho \bar{u}_i \bar{u}_j\right) = \rho f_i - \dfrac{\partial \bar{p}}{\partial x_i} + \dfrac{\partial}{\partial x_j}\left[\bar{\tau}_{ij} - \rho \overline{u_i' u_j'}\right] \end{cases} \quad \text{.....(1)}$$

Since there are more unknowns than equations, a strategy to "close" the system a is required. The feasible k-ε closure model is accurate for studying the velocity distribution of turbulent flow through a curved channel, according to Shaheed et al. [15]. It captures rotation, vortices, strong curvature of the streamline, and the unknown dissipation ε that incorporates the mean square fluctuation of the vorticity.

It is estimated by two equations (2) and (3):

- **The turbulent kinetic energy transport equation (k): :**

$$\frac{\partial}{\partial t}(\rho k) + \frac{\partial}{\partial x_j}(\rho k u_j) = \frac{\partial}{\partial x_j}\left[\left(\mu + \frac{\mu_t}{\sigma_k}\right)\frac{\partial k}{\partial x_j}\right] + P_k + P_b - \rho\varepsilon - Y_M \quad \text{.....} \quad (2)$$

Where the physical quantities are: density (ρ), mean velocity component (u_j), molecular dynamic viscosity (μ), turbulent viscosity (μ_t), turbulent Prandtl number for k (σ_k), production of k due to shear (P_k), production of k due to buoyancy (P_b), dissipation rate of k (), contribution of expansion in compressible flows (Y_M).

- **The dissipation rate transport equation (Ɛ) :**

$$\frac{\partial}{\partial t}(\rho\varepsilon) + \frac{\partial}{\partial x_j}(\rho\varepsilon u_j) = \frac{\partial}{\partial x_j}\left[\left(\mu + \frac{\mu_t}{\sigma_\varepsilon}\right)\frac{\partial \varepsilon}{\partial x_j}\right] + \rho C_1 S_\varepsilon - \rho C_{2\varepsilon}\frac{\varepsilon^2}{k + \sqrt{\nu_\varepsilon}} + C_{1\varepsilon}\frac{\varepsilon}{k}C_{3\varepsilon}P_b \quad (3)$$

Where the physical quantities are: Turbulent Prandtl number for ε (σ_ε), strain rate modulus S,

$$S = \sqrt{2S_{ij}S_{ij}} \text{ avec } S_{ij} = \frac{1}{2}\left(\frac{\partial u_i}{\partial x_j} + \frac{\partial u_j}{\partial x_i}\right) \text{ et } \nu = \frac{\mu}{\rho}$$

- **Closure: turbulent viscosity**
  - ✓ The turbulent viscosity is given by : $\mu_t = \rho C_\mu \dfrac{\kappa^2}{\varepsilon}$
  - ✓ $C_1 = \max\left[0.43, \dfrac{\eta}{\eta+3}\right]$, $\eta = S\dfrac{k}{\varepsilon}$, $\tau_{ij} = -\dfrac{2}{3}\rho k\delta_{ij} + 2\mu_t S_{ij}$
  - ✓ C_μ depends on the flow, it is not constant : $C_\mu = \dfrac{1}{A_0 + A_S\dfrac{k}{\varepsilon}s}$
  - ✓ With $A_0 = 4.04$ et $A_S = \sqrt{6}\cos\phi$, which depends on the local structure of the flow

$$\phi = \frac{1}{3}\cos^{-1}\left(\sqrt{6}\frac{S_{ij}S_{jk}S_{ki}}{\tilde{S}^3}\right); \tilde{S} = \sqrt{S_{ij}S_{ij}}\,; C_\mu = 0.09\,; C_{1\varepsilon} = 1.44\,; C_{2\varepsilon} = 1.9\,; \sigma_k = 1.0\,; \sigma_\varepsilon = 1.2$$

- **The energy conservation equation can be expressed as follows::**

$$\frac{\partial T}{\partial t}+\frac{\partial}{\partial x_j}\left(T\bar{u}_j\right)=\frac{\partial}{\partial x_j}\left(\lambda_{eff}\frac{\partial T}{\partial x_j}\right) \quad (4)$$

In Eq. (4):

- ✓ T represents the temperature,
- ✓ λ_{eff} is an effective coefficient that includes the contribution of turbulent mixing in addition to molecular conduction and can be expressed as: $\lambda_{eff}=\lambda+\frac{\mu_t Cp}{\mathrm{Pr}_t}$, where k and Cp are the thermal conductivity and specific heat at constant fluid pressure and μt is the turbulent viscosity.
- ✓ Pr_t is a turbulent Prandtl number, we will take: Pr_t= 0.85.

3. Numerical Modeling and Validation:

Since it is virtually impossible to obtain an exact analytical solution to the equations of our problem, we will resort to a numerical solution. The finite volume method was used [16]. It is more economical in terms of volume and computation time while ensuring high computational stability and is more efficient than classical finite difference methods for complex geometry problems. We opted for the QUICK scheme to discretize the convective terms. It minimizes numerical diffusion effects and is renowned for its accuracy in representing gradients, and is particularly effective for turbulent flows and high gradients. For the pressure-velocity coupling, we chose the coupled scheme [16]. Numerical tests are performed with convergence threshold residuals for the continuity, motion, k-epsilon, and energy equations equal to 10^{-6} in order to address both speed, accuracy, and better convergence of the calculations. Mesh independence was investigated and found to be satisfactory. We performed the numerical solution using Ansys Fluent 2024R2.
Thanks to a satisfactory comparison with results of Wang Fuzhang et al. [11] and we validated our work.

4. Analysis and discussion of results

Each inlet, whether hot or cold, has its own characteristics (section, temperature and speed, etc.), which implies distinct physical properties depending on the cases studied: case I (InV_1= InV_2= InV_3 = 3), case II (InV_1 =10; InV2 = InV_3 =3) and case III (InV_1 =3; InV2 = InV_3 =10). These differences are reflected in particular by potential variations in the mass flow rate and the total heat transfer rate for each inlet, which directly influences the flow dynamics and the heat transfer phenomena in the duct. Tables 2 and 3 present the mass flow rate and the total heat transfer rate for each inlet of each case for air and water.

Table 2 Mass flow rate [kg/s]

	Case (Inlet Velocities [m/s])	Inlet 1 [kg/s]	Inlet 2 [kg/s]	Inlet 3[kg/s]
Motion of air	**Case I** $InV_1 = InV_2 = InV_3 = 3$	0.00461814120078	0.00461814120078	0.00461814120078
Motion of water		3.763125344176	3.763125344176	3.763125344176
Motion of air	**Case II** InV_1=10; $InV_2 = InV_3$ =3	0.01539380400259	0.00461814120078	0.00461814120078
Motion of water		12.5437511472533	3.763125344176	3.763125344176
Motion of air	**Case III** $InV1$=3; $InV_2 = InV_3$ = 10	0.00461814120078	0.01539380400259	0.01539380400259
Motion of water		3.763125344176	12.5437511472533	12.5437511472533

The meeting of the jets from the three inlets or the addition of their physical quantities creates shocks or collisions in the mixing zone of the junction which will generate strong hydrodynamic and thermal interactions, disturbances and turbulence in the conduit. To evaluate and study its effects, the velocity, temperature distribution and turbulent kinetic energy profiles in the plane (x,y,z=0) and at sections CS1 (i.e., the circular surface 30 mm after mixing), CS2 (i.e., another circular surface 100 mm from the mixing domain) and CS3 (i.e., the circular outlet surface, located 20 mm after the duct bend) with three cases: case I (InV_1= InV_2= InV_3 = 3), case II (InV_1 =10 ; InV_2 = InV_3 =3) and case III (InV_1 =3 ; InV_2 = InV_3 =10) are presented according to the contours (Figure 2-19).

Table 3 Total heat transfer rate at the inlets [W]:

	CaseInlet Velocities [m/s]	Inlet 1 [W]	Inlet 2[W]	Inlet 3[W]
Motion of air	**Case I** $InV_1 = InV_2 = InV_3 = 3$	23.23917924349	-92.9567169739598	-92.9567169739598
Motion of water		78,686.9509467201	-314,747.80378688	-314,747.80378688
Motion of air	**Case II** InV_1=10; $InV_2 = InV_3$ =3	77.4639308116332	-92.9567169739598	-92.9567169739598
Motion of water		262,289.836489067	-314,747.80378688	-314,747.80378688
Motion of air	**Case III** InV1=3; $InV_2 = InV_3$ = 10	23.23917924349	-309.855723246533	-309.855723246533
Motion of water		78,686.9509467201	-1,049,159.34595627	-1,049,159.34595627

The fluid velocity appears to increase along the radial direction, with the maximum velocity occurring at the pipe axis (Figure 2-7). At the intersection, the horizontal jet is disturbed by the two inclined jets from the two inlets (inlet 2 and inlet 3). This causes velocity gradients (increased local velocity, intense mixing with high turbulence) and vortices in the mixing zone at the center of the junction. Flow acceleration is observed after the junction (mixing zone) and before the bend. At the bend, its centrifugal effect causes the peak velocity to be deflected toward the outer wall of the bend and decelerated toward the inner wall. When a fluid moves from a straight path toward a curved pipe (180° bend), the flow appears to be subject to a centrifugal force that pulls the fluid outward. This is compounded by a radial pressure variation that attempts to compensate for this centrifugal force. It creates transverse instability and generates secondary flows, in addition to the main flow. These secondary flows form two counter-rotating vortices called Dean vortices. Hence, the increase or maximization of velocity at the inner wall of the bend is due to the secondary movement (Dean vortex). The opposite effect occurs when the fluid leaves the bend towards the straight pipe. At the outer wall, the area with the largest radius, friction is greater, which can also lead to a slowdown.

The turbulent flow speed of air and water through sections CS1 and CS2 appears to be almost identical for cases 1 (Figs. 2 and 3). They show an increasingly homogeneous distribution of velocity, higher in the center. In CS2, the effect of the bend begins to be felt with the decrease in velocity at the bottom. In CS3, after the bend the minimum velocity is rejected towards the inner wall (blue spot at the bottom which enlarges), the maximum velocity is rejected towards the outer wall, which is due to the recirculation of the fluid in the bend (Dean vortex effect). For Case II (InV1 = 10; InV2 = InV3 = 3), the mass flow rate of inlet 1 is higher than that of inlets 2 and 3. The collision of the latter two with the first is not strong enough to disturb it, hence the mixing zone of the junction is less agitated (Figure 4,5). The velocities in CS1 and CS2 are higher than those in Case I because its mass flow rate from inlet 1 is greater and more imposing. The effect of the U-bend will be felt in CS3. For Case III (InV1 = 3; InV2 = InV3 = 10), the cumulative mass flow rates of the three inlets are greater than those in Cases II and I, leading to much stronger collisions and much steeper velocity gradients, resulting in increased turbulence (Figure 6,7). The velocities in CS1 and CS2 are more significant than those in Cases I and II. The effects of the secondary flow of the Dean vortex are more pronounced in case III, followed by case II and case I. We have a better hydrodynamic mixing respectively for case III, case II, and case I. The blue spot at the bottom (slow fluid) on CS3 is much more significant for air than for water and much more persistent respectively for cases I, followed by case II and case III (hydrodynamic mixing). This is due to the fact that hydrogen bonds are more present in water than in air (the dynamic viscosity of water is greater than that of air).

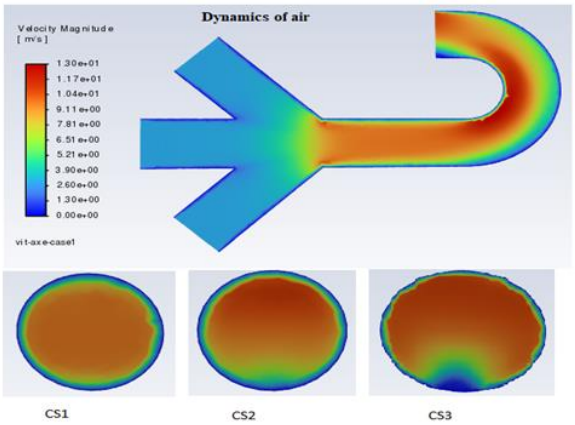

Figure 2 Velocity distribution across the domain of air dynamics - Case I (InV_1= InV_2= InV_3 = 3).

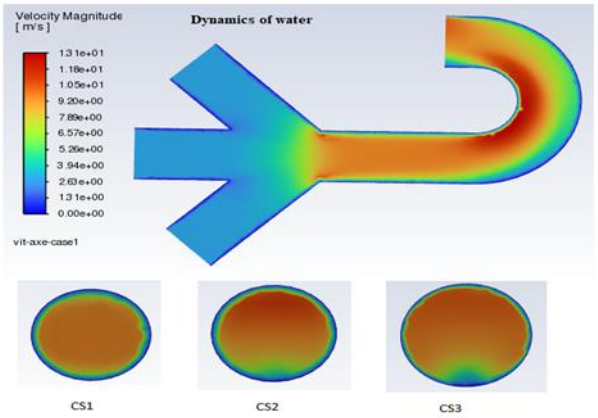

Figure 3 Velocity distribution across the domain of water dynamics - Case I(InV_1= InV_2= InV_3 = 3).

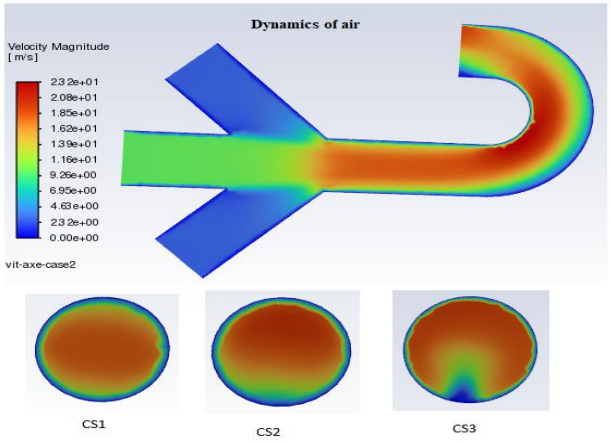

Figure 4 Velocity distribution across the domain of air dynamics - Case II (InV_1 =10 ; InV_2 = InV_3 =3).

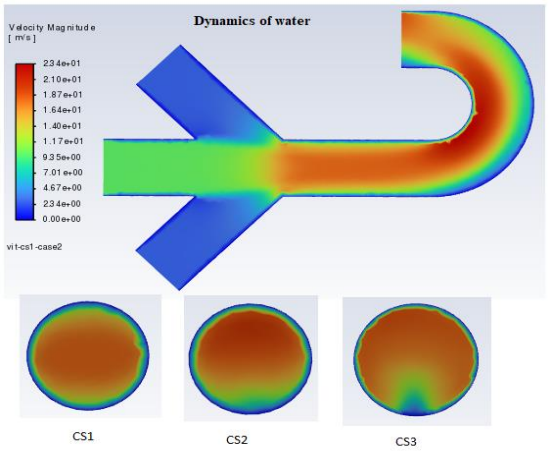

Figure 5 Velocity distribution across the domain of water dynamics - Case II (InV_1 =10 ; InV_2 = InV_3 =3).

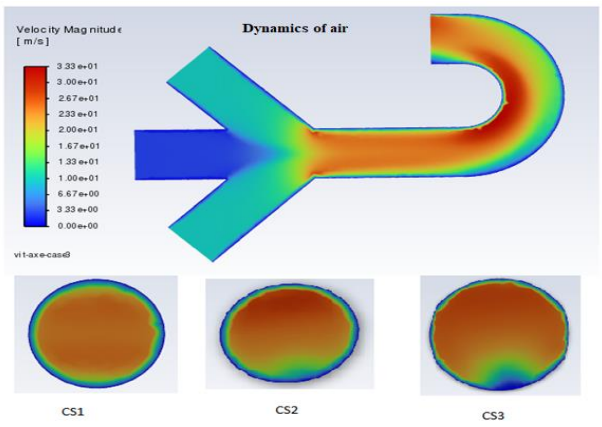

Figure 6 Velocity distribution across the domain of air dynamics - Case III (InV_1 =3 ; InV_2 = InV_3 =10).

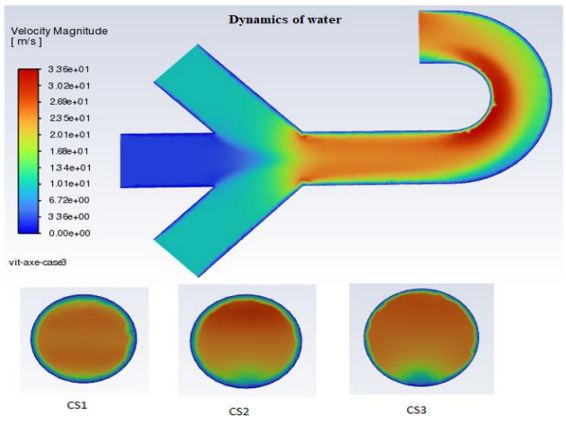

Figure 7 Velocity distribution across the domain of water dynamics - Case III (InV_1 =3 ; InV_2 = InV_3 =10).

Figure 8-13 shows the hot flow inlet 1 and the other two inlets (inlet 2 and inlet 3) which carry cold fluid. With the meeting of the cold flows on the hot flow, a clear thermal transition zone called cold fronts are formed and emerge from the mixing zone of the junction along the axis of the duct in the three cases (Case I, Case II and Case III). This formation of visible cold fronts is very important in the mixing domain. This is due to the significant changes observed in the temperature distribution with the velocities of each inlet.

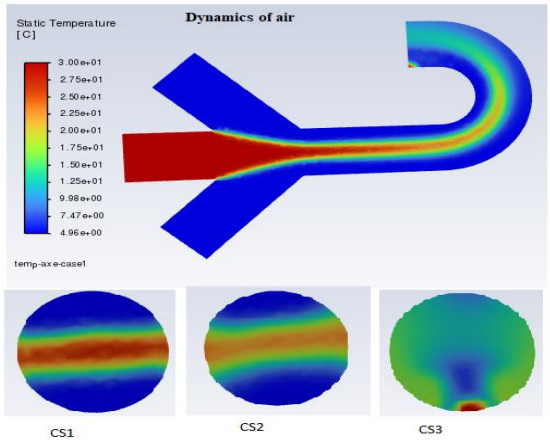

Figure 8 Temperature distribution across the domain of air dynamics - Case I (InV_1= InV_2= InV_3 = 3)..

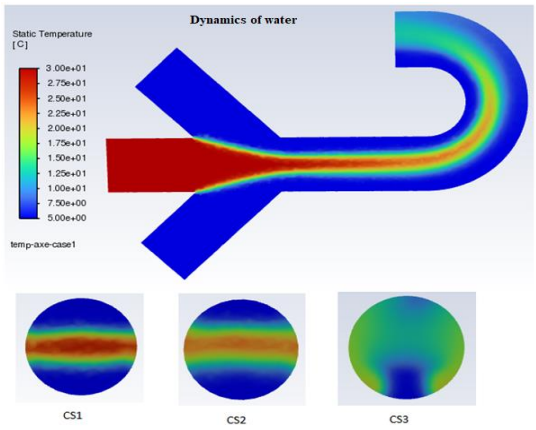

Figure 9 Temperature distribution across the domain of water dynamics - Case I (InV_1= InV_2= InV_3 = 3).

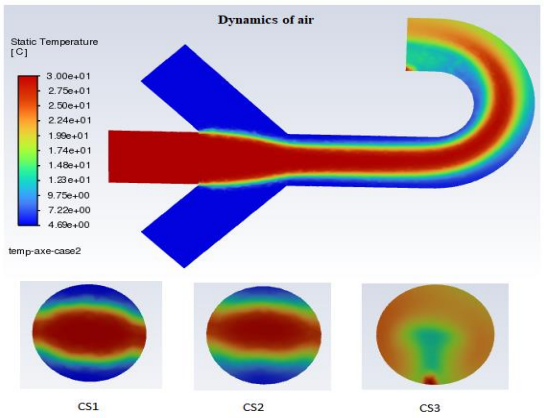

Figure 10 Temperature distribution across the domain of air dynamics - Case II (InV_1 =10 ; InV_2 = InV_3 =3).

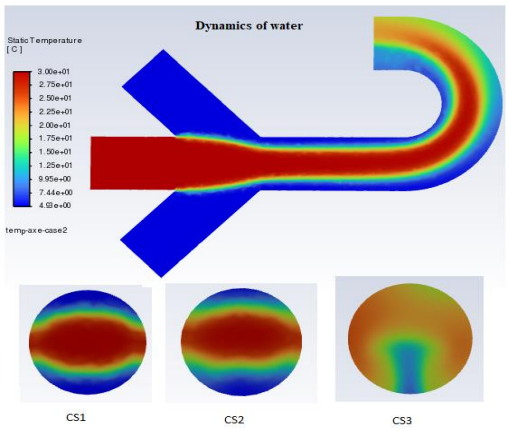

Figure 11 Temperature distribution across the domain of water dynamics - Case II (InV_1 =10 ; InV_2 = InV_3 =3).

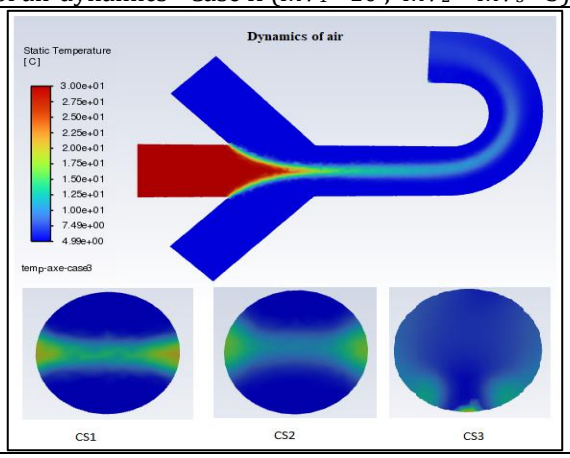

Figure 12 Temperature distribution across the domain of air dynamics - Case III (InV_1 =3 ; InV_2 = InV_3 =10).

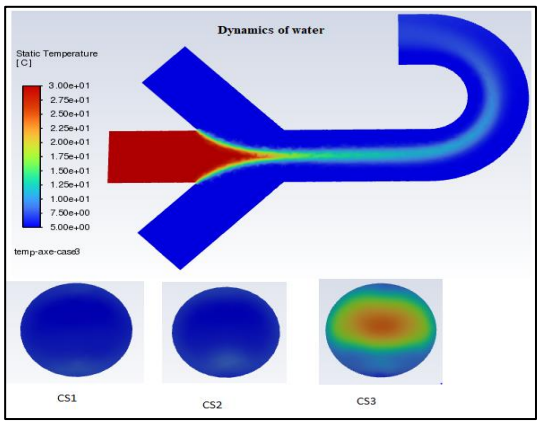

Figure 13 Temperature distribution across the domain of water dynamics - Case III (InV_1 =3 ; InV_2 = InV_3 =10).

For Case I (InV1= InV2= InV3 = 3), the velocities of the cold flows are equal to those of the hot ones, we have a more moderate and controlled collision (Figure 8,9). For Figure 10, 11 (Case II (InV1 =10; InV2 = InV3 =3)), the heat of the hot flow from inlet 1 is more imposing, so the temperature is little disturbed around the axis of the duct even after the collision at the mixing zone. There is a dominance of the hot in the central zone, on the axis of the duct and a progressive cooling in the lateral zones. For Figure 12, 13 (Case III (InV1 =3; InV2 = InV3 =10)), the hot flow from inlet 1 is weak compared to the two cold flows, so thinner or weakened around the axis of the duct.

Cold dominates the pipe. For all three cases (case I, case II, and case III), we observe that in CS2, the temperature is significantly more homogeneous than in CS1. The bend triggered a secondary flow (Dean vortex) that favored transverse mixing. However, the low velocity of the cold fluid (air and water) at inlets 2 and 3 creates a prolonged cold front reaching the circular surface CS2 before curving (example for case I) and can even reach the circular surface CS3 at the outlet (for case II) when the velocity of inlet 1 is high. We observe a small red peak (temperature maximum) at the pipe outlet, in CS3 for air and differently for water in both cases (case I and case II), which coincides with cases where the prolonged cold front is favored. Thermally, water is more orderly, its thermal capacity and thermal conductivity are higher than those of air, meaning that it absorbs more heat without sudden temperature variations and transmits thermal energy more quickly than air in a more homogeneous manner thanks to its density (water molecules are closer to each other, collisions are more frequent).

Figure 14-19 shows the distribution contours of turbulent kinetic energy. It is the amount of energy per unit mass contained in the turbulent (random) motions of the flow and quantifies the level of disorder of the local vortical motion and the intensity of turbulence in the flow. Zero turbulent kinetic energy at the three inlets implies a more ordered or laminar flow regime. At the junction, we find that it is low for case I (Figure 14, 15) and higher for cases III (Figure 18, 19) followed by case II (Figure 16, 17). This is due to the interference of jets with possibly different speeds creating strong velocity gradients and a high shear rate. Despite this, Y-junctions generate less intense, more moderate and more controlled turbulence than T-junctions due to the non-perpendicular collision of the jets which promotes flow continuity and a smoother transition. The turbulent kinetic energy begins to increase just before the bend, increases progressively in the bend and reaches its maximum at the end of the bend. The bend is the main source of turbulence production in the duct. The U-bend generates more disruptive hydrodynamic effects than those induced by the Y junction, due to centrifugal forces and more intense recirculations (Dean vortex). The turbulent kinetic energy is low in CS1 and CS2 and higher in CS3 (U-bend effect). It can be clearly seen that the water flows are intensely more turbulent. This is mainly explained by its higher density and lower kinematic viscosity.

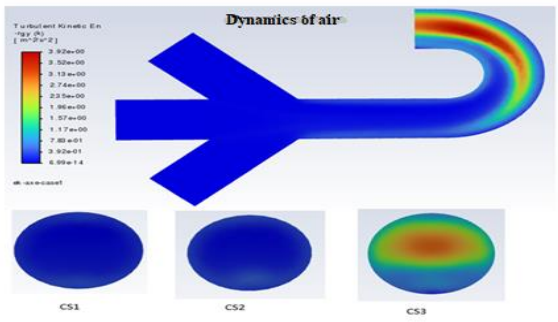

Figure 14 Turbulent kinetic energy across the domain of air dynamics - Case I (InV_1= InV_2= InV_3 = 3).

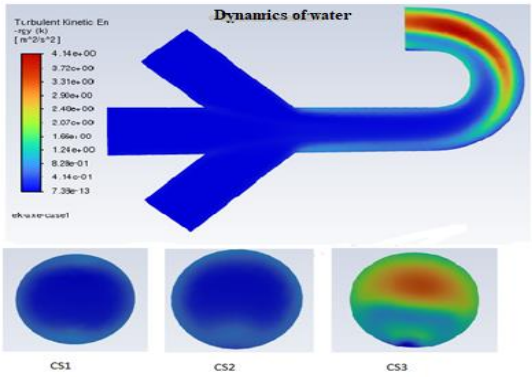

Figure 15 Turbulent kinetic energy across the domain of water dynamics - Case I (InV_1= InV_2= InV_3 = 3).

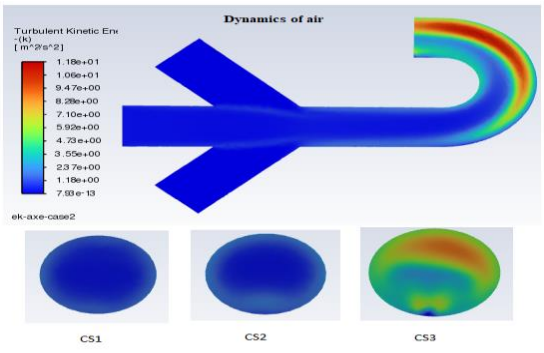

Figure 16 Turbulent kinetic energy across the domain of air dynamics - Case II (InV_1 =10 ; InV_2 = InV_3 =3).

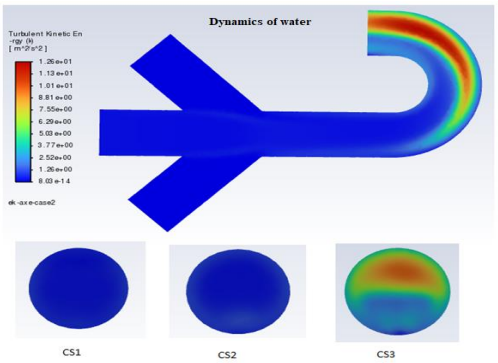

Figure 17 Turbulent kinetic energy across the domain of water dynamics - Case II (InV_1 =10 ; InV_2 = InV_3 =3).

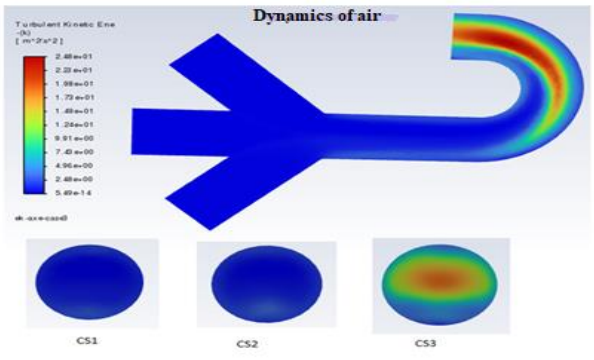

Figure 18 Turbulent kinetic energy across the domain of air dynamics - Case III (InV_1 =3 ; InV_2 = InV_3 =10).

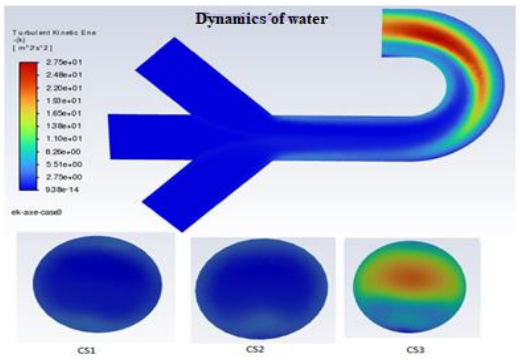

Figure 19 Turbulent kinetic energy across the domain of water dynamics - Case III (InV_1 =3 ; InV_2 = InV_3 =10).

Nomenclature

Latin letters

- *Cp: Specific Heat, J/(Kg.K)*
- *D :* Main pipe diameter, m
- g : Acceleration of gravity, $m.s^{-2}$
- K: kinetic energy of turbulence, $m^2.s^{-2}$
- *P:* Pressure, Pa
- S_{ij} :Strain rate tensor
- t : Time, s
- $\overline{T}$: Filtered temperature, K^{-1}
- u, v, w : Velocity components, $m.s^{-1}$
- u', v', w': Fluctuating velocity components, $m.s^{-1}$
- $\overline{u}_i$: Filtered velocity component in x_i direction, $m.s^{-1}$
- u_τ : Parietal Friction Velocity
- *x, y, z:* Cartesian coordinates, m
- *Pr:* Laminar Prandtl number
- Pr_t : Turbulent Prandtl number

Greek letters

- α : Thermal diffusivity, $m^2.s^{-1}$
- β : Coefficient of thermal expansion, K^{-1}
- λ: Thermal conductivity, $W.m^{-1}.K^{-1}$
- ν: Kinematic viscosity, $m^2.s^{-1}$
- ρ : Density, $kg.m^{-3}$
- μ: Dynamic viscosity, $kg.m^{-1}.s^{-1}$
- α : Thermal diffusivity, $m^2.s^{-1}$
- σ_{ij}: Laminar stress tensor, Pa
- τ_{ij}: Subgrid scale stress tensor, Pa
- μ: Molecular dynamic viscosity, $kg.m^{-1}.s^{-1}$
- μ_t: Turbulent dynamic viscosity, $kg.m^{-1}.s^{-1}$
- ν: Molecular kinematic viscosity, $m^2.s^{-1}$
- ν_t: Turbulent kinematic viscosity, $m^2.s^{-1}$
- ε: Turbulence kinetic energy dissipation rate, $m^2.s^{-3}$

5. Conclusion

This work examines the dynamics of air and water flowing through a Y-junction duct with three inlets followed by a U-bend, with particular attention paid to the cold front phenomenon. The study analyzes the behavior of these fluids (air and water) at various key positions: at the duct axis, 70 mm from the mixing zone (CS1), just upstream of the bend (CS2), and downstream, at the outlet (CS3). The results show:

- Water transfers thermal energy more efficiently and orderly than air due to its higher density, promoting more frequent collisions, and its higher specific heat capacity and thermal conductivity, allowing it to store and transport more energy without sudden temperature changes.
- The best hydrodynamic mixing is obtained for Case III, Case II, and Case I, respectively, in descending order of the cumulative mass flow rates of the three inlets (highest collision).
- Three cases of cold front formation were examined, considering the variation in inlet velocity. The low velocity of the cold fluid (air and water) at inlets 2 and 3 generates an extensive cold front, which can even extend as far as the circular surface CS2 (case I) and sometimes even as far as the circular surface CS3 at the outlet of the duct when the velocity at inlet 1 is high (case II).
- The U-bend generates more disruptive hydrodynamic effects than those induced by the Y junction. The U-bend acts as a turbulence amplifier, but the response of the fluid (air and water) depends on its physical properties (its density, especially its kinematic viscosity, etc.).
- The complexity of the dynamics of water and air in a flow with a U-bend is not only explained by mechanical phenomena (turbulence, recirculation, etc.) but also by the physicochemical characteristics specific to each fluid. Water has a polar molecular structure capable of forming hydrogen bonds, which can be influenced by the presence of cold fronts, unlike air, which is a mixture of non-polar gases with few strong intermolecular interactions.

Compliance with ethical standards

Disclosure of conflict of interest

No conflict of interest to be disclosed.

References

[1] A.S Athulya, C. R. Miji, 'CFD modelling of multiphase flow through T junction', *International Conference on Emerging Trends in Engineering, Science and Technology (ICETEST 2015*), Procedia Technology 24, pp 325 – 331, 2016..

[2] Mr.G.B. Nimadge, Mr.S.V. Chopade, 'CFD analysis of flow through t-junction of pipe', International Research Journal of Engineering and Technology (IRJET) Volume:4 Issue:2, pp. 906-911, Feb-2017.

[3] W. Khan, A. K. Chandra, K. Kishor , S. Sachan, M. S. Alam, 'Slug formation mechanism for air–water system in T-junction microchannel: a numerical investigation', Chemical Papers, 72(11), 2921–2932, (2018). https://doi.org/10.1007/s11696-018-0522-7

[4] Y. Doroshenko, J. Doroshenko, V. Zapukhliak, L. Poberezhny, P. Maruschak, 'Modeling computational fluid dynamics of multiphase flows in elbow and t-junction of the main gas pipeline', TRANSPORT, Volume 34 Issue 1, pp. 19–29, 2019. https://doi.org/10.3846/transport.2019.7441

[5] A. M. RAID, CFD instraction guide to simulate two-phase flow separation in a vertical T-junction separator. International Journal of Advances in Science Engineering and Technology, Vol-7, Iss-2, Spl. Issue-1 May-2019.

[6] Chiriac Eugen, Diana Broboana, Marioara Avram, Corneliu Balan, 'Comparative numerical study between OpenFOAM and ANSYS Fluent in a Y-junction microchannel', The 11th International Symposium on Advanced Topics in Electrical Engineering', March 28-30, 2019 Bucharest, Romania.

[7] M. A. Makarem, M. R. Kiani, M. Farsi M. R. Rahimpour, 'CFD Simulation of CO2 Capture in a Microchannel by Aqueous Mixtures of MEA and [Bmim] BF4 Modified with TiO2 Nanoparticles', International Journal of Thermophysics, Vol. 42 no. 4, (2021). https://doi.org/10.1007/s10765-021-02812-1

[8] E. S. Taha, M. A. Abdulwahid, A. M. A. Morad, Q. A. Maatooq, Computational Fluid Dynamic Analysis of the Flow though T-junction and Venturi Meter. Conference Paper ·IMDC-IST 2021, September 07-09, Sakarya, Turkey, pp. 1-9, Sept. 2021. http://dx.doi.org/10.4108/eai.7-9-2021.2314880

[9] M. Said, N. N. Bouda, S. Harmand, 'Numerical investigation of flow patterns and plug hydrodynamics in a 3D T-junction Microchannel', Research Square 2022. DOI:https://doi.org/10.21203/rs.3.rs-1613765/v1

[10] B. Khatoon, S. Ul Hasan, M. S. Alam, 'CO2 capturing in cross T-junction microchannel using numerical and experimental approach', Chemical Papers.- 77, pp. 6319–6340, July 2023. https://doi.org/10.1007/s11696-023-02941-x

[11] F. Wang, I. L. Animasaun, Q. M. Al-Mdallal, S. Saranya, T. Muhammad, 'Dynamics through three-inlets of t-shaped ducts: Significance of inlet velocity on transient air and water experiencing cold fronts subject to turbulence', International Communications in Heat and Mass Transfer, Vol. 148 (2023) 107034. https://doi.org/10.1016/j.icheatmasstransfer.2023.107034

[12] P. T. Ndiaye & O. N. Thiam, 'Computational fluid dynamics analysis of the influence of velocity at inlet 2 on heat transfer and fluid flow in the mixing elbow', Journal of Scientific and Engineering Research, vol. 11 no. 2, pp. 93-101, 2024.

[13] P. T. Ndiaye & O. N. Thiam, 'Computational Fluid Dynamics Analysis of the Influence of Diameter at Inlet 2 on Heat Transfer and Fluid Flow in the Mixing Elbow'. Journal of Applied Physical Science International, vol. 15 no. 2, pp. 61–70. https://doi.org/10.56557/japsi/2023/v15i28552.

[14] T.-H. Shih, W.W. Liou, A. Shabbir, Z. Yang, J. Zhu, 'A new k-ε eddy viscosity model for high Reynolds number turbulent flows', Comput. Fluids vol. 24 no. 3 pp. 227–238, 1995. https://doi.org/10.1016/0045-7930(94)00032-t.

[15] R. Shaheed, A. Mohammadian, G. H. Kheirkhah, 'A comparison of standard k-e and realizable k-e turbulence models in curved and confluent channels, Environ', Fluid Mech, Vol. 19 no. 2, pp. 543–568, 2019. https://doi.org/10.1007/s10652-018-9637-1.

[16] H. K. Versteeg, and W. Malalasekera, An Introduction to Computational Fluid Dynamics: The Finite Volume Method, 2nd ed. Harlow, England: Pearson Education, 2007.